We are IntechOpen, the world's leading publisher of Open Access books
Built by scientists, for scientists

6,000
Open access books available

148,000
International authors and editors

185M
Downloads

154
Countries delivered to

Our authors are among the

TOP 1%
most cited scientists

12.2%
Contributors from top 500 universities

CLARIVATE ANALYTICS
BOOK CITATION INDEX
INDEXED

WEB OF SCIENCE™

Selection of our books indexed in the Book Citation Index
in Web of Science™ Core Collection (BKCI)

Interested in publishing with us?
Contact book.department@intechopen.com

Numbers displayed above are based on latest data collected.
For more information visit www.intechopen.com

Chapter

Anomalous Charge Transport Properties and Band Flattening in Graphene: A Quasi-Relativistic Tight-Binding Study of Pseudo-Majorana States

Halina V. Grushevskaya and George Krylov

Abstract

Anomalous charge carrier transport in graphene is studied within a topologically nontrivial quasi-relativistic graphene model. The model predicts additional topological contributions, such as the Majorana-like mass-term correction to the ordinary ohmic component of the current, the spin-orbital-coupling, "Zitterbewegung"-effect corrections to conductivity in space, and time dispersion regime. The corrections appear due to non-Abelian quantum statistics for the charge carriers in graphene. The chiral anomaly of electrophysical and optical properties may emerge due to a deconfinement of the pseudo-Majorana quasiparticles. It has been shown that phenomena of negative differential conductivity, loss of universal far-infrared optical conductivity, and nonzero "minimal" direct-current conductivity in graphene occur due to flattening and vorticity of the pseudo-Majorana model graphene energy bands.

Keywords: graphene, anomalous charge transport, conductivity, chiral anomaly, quasi-relativistic model, Dirac-Hartree-Fock self-consistent field approximation, pseudo-Majorana fermion graphene model

1. Introduction

Graphene discovery is the driving force for progress in the current developments of quantum devices due to fascinating electrical and optical graphene properties. Graphene is an atomically thin carbon layer, in which valent and conduction bands touch each other in six points of hexagonal Brillouin zone, called Dirac points or valleys K, K' [1]. Graphene belongs to strongly correlated systems, in which many-body interactions occur. Thanks to the strong electron-hole correlations, the electrophysical and optical properties of the graphene are very unusual. According to the linear response theory, the temperature dependence of the Hall conductivity for Fermi liquid, to which most metals belong, does not depend upon temperature [2]. But, the strongly correlated systems exhibit an anomalous charge magnetotransport

[3]. A similar situation prevails for universal nonzero direct-current (DC) graphene minimum conductivity (scale range of $\frac{4e^2}{h}$ [4] – $\frac{6e^2}{h}$ [5, 6] depending on support type) when the linear response theory predicts vanishing electrical conductivity for direct current (DC) or $\frac{4e^2}{\pi h}$ for the low-frequency conductivity in pure graphene [7, 8]. Here, h is the Planck constant, and e is the electron charge.

The situation with optical conductivity in the far-infrared spectral range of $0.05 - 0.5$ eV ($25\,\mu$m–$350\,\mu$m) turned out to be even more unpredictable. Theoretical calculations of the far-infrared optical conductivity within a pseudo-Dirac massless fermion model for graphene predict its universal value, $\frac{e^2}{4h}$, [9], which contradicts entirely experimental data on the existence of extrema in this spectral range, namely, an asymmetric peak at 0.15 eV ($\sim 150 - 200$ cm^{-1}) [10] and a shallow minimum in the spectral range of $\sim 0.2 - 0.3$ eV [11, 12] (see **Figure 1a** and **b**). Here, $\hbar$ is the Planck constant divided by 2π. Slowly increasing the optical conductivity approaches the universal value in the mid-to-near-infrared spectral range of $0.5 - 1.2$ eV [13] where optical transitions occur far enough from the valleys K, K' of the graphene Brillouin zone. Thus, the applicability of the pseudo-Dirac graphene model is doubtful in both spectral ranges.

The electron is a complex fermion; thus, if one decomposes its wavefunction into its real and imaginary parts, which would be Majorana fermions, they are rapidly remixed by electromagnetic interactions. However, such a decomposition could be reasonable for graphene because of the effective electrostatic screening. Experimental signatures of graphene Majorana states in graphene-superconductor junctions without the need for spin-orbital coupling (SOC) have been established in [14]. An analysis of Majorana-like graphene models also become relevant in connection with the discovery of unconventional superconductivity for twisted bilayer graphene at $\theta \approx 1.05$ angle of rotation of one monoatomic layer (monolayer) relative to another one [15]. A quantum statistics of graphene model with Majorana-like states should be a non-Abelian one, and the absence of that is the main obstacle to shed light on topologically nontrivial mechanisms of graphene conductivity. The non-Abelian pseudo-Majorana statistics of graphene charge carriers, which could clarify the anomalous effects, are behind several major theoretical approaches to graphene. The approaches are based on the massless pseudo-Dirac fermion model. The pseudo-Dirac graphene model Hamiltonian gives predictions that are very different from experimental data for a wide range of transport phenomena in graphene physics, such as the existence of topological currents in graphene superlattices [16], a sharp rise of Fermi velocity value v_F in touching valent and conduction bands [17], and a lack of excitonic instability [18].

So, up to now, there is no consistent theory of topologically nontrivial graphene conductivity.

In this chapter, we show that charge transport coefficients in linear response to electromagnetic fields contain anomalous contributions arising from strong correlations between graphene charge carriers. The strong temperature dependencies that are observed in Hall, and optical and electrical conductivities are explained by non-Abelian statistics of topologically nontrivial graphene charge carriers of pseudo-Majorana nature within an earlier developed quasi-relativistic self-consistent Dirac-Hartree-Fock approach in a tight-binding approximation [19–25]. This quasi-relativistic approach allowed to achieve success in calculations of electronic properties for quasi-circular graphene $p - n(n - p)$ junctions also [26].

Our goal is to study quantum transport of charge carriers with vortex dynamics within a quasi-relativistic graphene model using a high-energy $\vec{k} \cdot \vec{p}$-Hamiltonian and
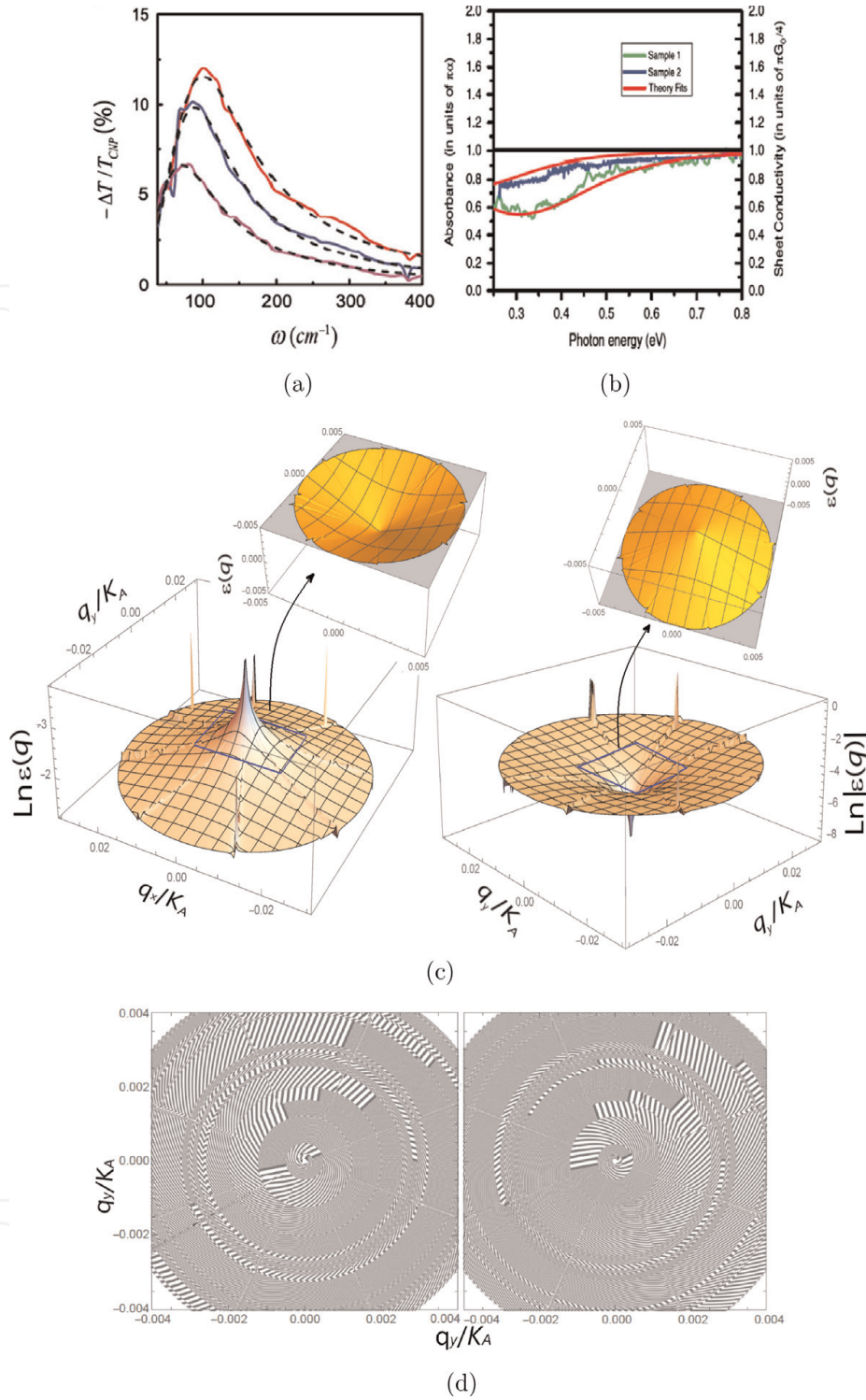
Figure 1.
Graphene conductivity and transmission spectra [10, 12] in the far-infrared (a) and mid-to-near-infrared (b) spectral ranges. Graphene conductivity is obtained from transmittance contrast. The normalized change $\Delta T/T_{CNP}$ in transmittance T_{CNP} of the non-dopped graphene is induced by the presence of the graphene sample; T_{CNP} is the transmittance at the applied voltage for charge-neutral Dirac point. The gate-induced change of transmission in graphene is obtained for different values of gate voltage. The Drude conductivity fitting is shown. (c) Electron (left) and hole bands (right) of a quasi-relativistic $N_F = 3$-flavors model graphene that were calculated with a pseudo-Majorana mass term. (d) The vortex texture in contour plots of electron (left) and hole (right) bands was calculated with the Majorana-like mass term on momentum scales $q/K_A = 0.002$; $\vec{q} = \vec{k} - \vec{K}$.

to perform simulations of the complex conductivity of the system in a number of experimentally interesting cases. The Wilson non-closed loop method will be used to prove dichroism of the band structure, which leads to valley Hall conductivity.

2. Fundamentals

Quasi-relativistic graphene model has been derived in [19] as a consequent account of the effect of relativistic exchange interactions, while being grounded on truly secondary quantized relativistic consideration of the problem within the known Dirac-Hartree-Fock self-consistent field approximation. In subsequent publications [23, 27, 28], it has been established that the model admits a form as a Majorana-like system of equations as well as a two-dimensional Dirac-like equation with an additional "Majorana-force correction" term [23]. It reads

$$v_F \left[\vec{\sigma}_{2D}^{AB} \cdot \vec{p}_{BA} - c^{-1} M_{BA} \right] |\psi_{BA}^*\rangle = E |\psi_{BA}^*\rangle \tag{1}$$

and the same equation with labels (AB, BA) exchanged for another sublattice. Here, (AB, BA) are related to sublattices and refer to the quantities that are obtained by similar transformations with a relativistic exchange matrix Σ_{rel}^x; for example, for the momentum operator $\vec{p}$ one gets $\vec{p}_{BA} = \Sigma_{BA} \vec{p} \, \Sigma_{BA}^{-1}$; v_F is the Fermi velocity. The vector of two-dimensional (2D) Pauli matrixes comprises two matrixes $\sigma_{2D} = (\sigma_x, \sigma_y)$. The term $M_{BA} = -\frac{1}{cv_F} \Sigma_{BA} \Sigma_{AB}$ is a Majorana-like mass term, where c is the speed of light. It turns out to be zero in the Dirac point $K(K')$ and gives a very small momentum-dependent correction outside of $K(K')$. The relativistic exchange operator for tight-binding approximation and accounting of nearest lattice neighbors is given by its action on secondary quantized wave functions on sublattices $A(B)$ of the system [19, 27, 28]

$$\Sigma_{rel}^x \begin{pmatrix} \hat{\chi}_{-\sigma_A \dagger} \left(\vec{r} \right) \\ \hat{\chi}_{\sigma_B}^\dagger \left(\vec{r} \right) \end{pmatrix} |0, -\sigma\rangle |0, \sigma\rangle$$

$$= \begin{pmatrix} 0 & \Sigma_{AB} \\ \Sigma_{BA} & 0 \end{pmatrix} \begin{pmatrix} \hat{\chi}_{-\sigma_A}^\dagger \left(\vec{r} \right) \\ \hat{\chi}_{\sigma_B}^\dagger \left(\vec{r} \right) \end{pmatrix} |0, -\sigma\rangle |0, \sigma\rangle, \tag{2}$$

$$\Sigma_{AB} \hat{\chi}_{\sigma_B}^\dagger \left(\vec{r} \right) |0, \sigma\rangle = \sum_{i=1}^{N_v N} \int d\vec{r}_i \hat{\chi}_{\sigma_i B}^\dagger \left(\vec{r} \right) |0, \sigma\rangle \Delta_{AB}$$

$$\left\langle 0, -\sigma_i \left| \hat{\chi}_{-\sigma_i^A}^\dagger \left(\vec{r}_i \right) V \left(\vec{r}_i - \vec{r} \right) \hat{\chi}_{-\sigma_B} \left(\vec{r}_i \right) \right| 0, -\sigma_{i'} \right\rangle, \tag{3}$$

$$\Sigma_{BA} \hat{\chi}_{-\sigma_A \dagger} \left(\vec{r} \right) |0, -\sigma\rangle = \sum_{i'=1}^{N_v N} \int d\vec{r}_{i'} \hat{\chi}_{-\sigma_{i'}^A \dagger} \left(\vec{r} \right) |0, -\sigma\rangle \Delta_{BA}$$

$$\left\langle 0, \sigma_{i'} \left| \hat{\chi}_{\sigma_B^B}^\dagger \left(\vec{r}_{i'} \right) V \left(\vec{r}_{i'} - \vec{r} \right) \hat{\chi}_{\sigma_A} \left(\vec{r}_{i'} \right) \right| 0, \sigma_i \right\rangle. \tag{4}$$

Here, interaction (2×2)-matrices Δ_{AB} and Δ_{BA} are gauge fields (or components of a gauge field). Vector-potentials for these gauge fields are introduced by the phases α_0 and $\alpha_{\pm,k}$, $k = 1, 2, 3$ of $\pi(p_z)$-electron wave functions $\psi_{p_z}(\vec{r})$ and $\psi_{p_z,\pm\vec{\delta}_k}(\vec{r})$ attributed to a given lattice site and its three nearest neighbors (see details in [28]), $V(\vec{r})$ is the three-dimensional (3D) Coulomb potential, and the summation is performed on all lattice sites and number of electrons. The introduction of these three non-Abelian gauge fields was stipulated by a requirement of the reality of eigenvalues of the Hamiltonian operator as gauge conditions. In this case, the operator of relativistic exchange gains an additional implicit $\vec{k}$-dependence upon momentum in the case of nonzero values of gauge fields.

3. Electronic structure

The band structure of graphene within the quasi-relativistic $N_F = 3$-flavors model has been calculated (see [25] and references therein) with the Majorana-like mass term and is presented in **Figure 1c**. The graphene bands are conical near the Dirac point at $q(q') \to 0$, $q = \left|\vec{p} - \vec{K}\right|$ ($q' = \left|\vec{p}' - \vec{K}'\right|$) where $\vec{p}$ ($\vec{p}'$) is a momentum of electron (hole). But, they flatten at large $q(q')$. The band structure of graphene within the quasi-relativistic model with pseudo-Majorana charge carriers hosts vortex and antivortex whose cores are in the graphene valleys $\vec{K}$ and $\vec{K}'$ of the Brillouin zone, respectively (**Figure 1c** and **d**). Touching the Dirac point $K(K')$, the cone-shaped valence and conduction bands of graphene are flattened at large momenta p of the graphene charge carriers [23]. It signifies that the Fermi velocity v_F diminishes drastically to very small values at large momenta p. Since eight sub-replicas of the
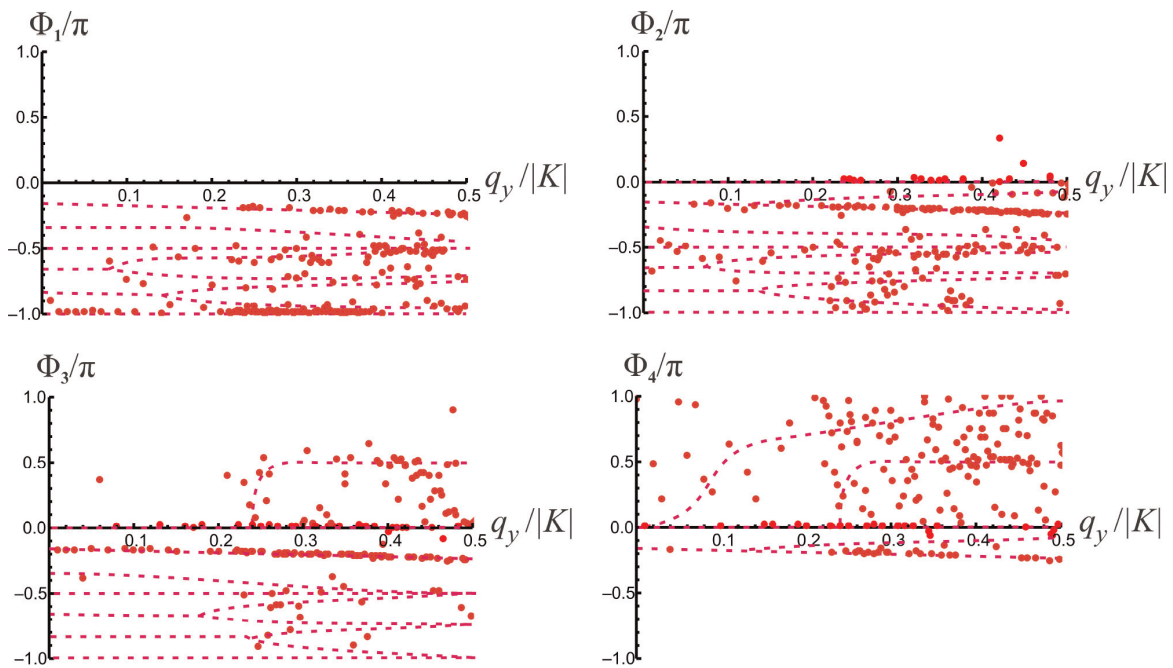

Figure 2.
Non-Abelian phases $\Phi_1, \ldots, \Phi_4$ of the Wilson loop eigenvalues in the units of π at nonzero gauge fields; $\vec{q} = \vec{k} - \vec{K}$.

graphene band near the Dirac point degenerate into the eightfold conic band (**Figure 1c** and **d**) the pseudo-Majorana fermions forming the eightfold degenerate vortex are confined by the hexagonal symmetry. In the state of confinement, the pseudo-Majorana fermions are linked with the formation of electron-hole pairs under the action of the hexagonal symmetry.

A global characterization of all Dirac touching with non-Abelian Zak phases $\Phi_1, \Phi_2, \Phi_3, \Phi_4$ as arguments of the Wilson loop operator for our model is presented in **Figure 2** [23]. Accordingly, in the case of the nonzero gauge fields, the simulations predict the homotopy group Z_{12} with the generator $-\pi/6$ in the Dirac points $K(K')$ [23]. **Figure 1d** shows that the proposed model has the nontrivial topological properties revealing in the dichroism of its band structure. The vorticity of the band is originated from Majorana-like excitations. It is natural to assume that such peculiarities would lead also to observable consequences in charge transport in such a system.

4. Non-Abelian currents in quasi-relativistic graphene model

Conductivity can be considered as a coefficient linking the current density with an applied electric field in a linear regime of response. To reach the goal, several steps should be performed. First, one has to subject the system to an electromagnetic field, and this can be implemented by a standard change to canonical momentum $\vec{p} \to \vec{p} - \frac{e}{c}\vec{A}$ in the Hamiltonian in the following way:

$$\left[c\vec{\sigma}_{2D}^{BA} \cdot \left(\vec{p}_{AB} - \frac{e}{c}\vec{A} \right) - \Sigma_{AB}\widetilde{\Sigma}_{BA}\left(\vec{p}_{AB} - e\vec{A}/c \right) \right] \widehat{\widetilde{\chi}^{\dagger}_{+\sigma_B}}\left(\vec{r} \right) \left| 0 - \sigma \right\rangle = cE_{qu}(p)\widehat{\widetilde{\chi}^{\dagger}_{+\sigma_B}}\left(\vec{r} \right) \left| 0, - \sigma \right\rangle,$$

$$\Sigma_{AB}\widetilde{\Sigma}_{BA}\left(\vec{p}_{AB} - e\vec{A}/c \right) = \Sigma_{AB}\widetilde{\Sigma}_{BA}(0) + \sum_i \frac{d\Sigma_{AB}\widetilde{\Sigma}_{BA}}{dp_i'}\Big|_{p_i'=0} \left(p_i^{AB} - \frac{e}{c}A_i \right)$$

$$(5)$$

$$+ \frac{1}{2}\sum_{i,j} \frac{d^2\Sigma_{AB}\widetilde{\Sigma}_{BA}}{dp_i'dp_j'}\Big|_{p_i', \ p_j'=0} \left(p_i^{AB} - \frac{e}{c}A_i \right)\left(p_j^{AB} - \frac{e}{c}A_j \right) + \dots. \quad (6)$$

Here, $\vec{A}$ is a vector potential of the field. In what follows, we omit the cumbersome designation "AB" if this does not lead to a lack of sense.

Second, to find the quasi-particle current we use the perturbation theory [29, 30]. Taking into account the expression (6), a potential energy operator V for interaction between the secondary quantized fermionic field $\chi_{+\sigma_B}(x)$ with the electromagnetic field reads

$$V = \chi^{\dagger}_{+\sigma_B} \left[-c\vec{\sigma}_{BA} \cdot \frac{e}{c}\vec{A} - M_{BA}(0) - \sum_i \frac{dM_{BA}}{dp_i'}\Big|_{p_i'=0} \times \left(p_i^{AB} - \frac{e}{c}A_i \right) \right. \quad (7)$$

$$\left. - 12\sum_{i,j} \frac{d^2M_{BA}}{dp_i'dp_j'}\Big|_{p_i', \ p_j'=0} \times \left(p_i^{AB} - \frac{e}{c}A_i \right)\left(p_j^{AB} - \frac{e}{c}A_j \right) + \dots \right] \chi_{+\sigma_B}.$$

Then, one can find a quasi-relativistic current [31] of charge carriers in graphene as:

$$
\begin{aligned}
j_i^{SM} &= c^{-1}j_i \equiv j_i^O + j_i^{Zb} + j_i^{so}, \\
j_i &= e\chi_{+\sigma_B}^{\dagger}(x^+)v_{x^+x^-}^i\chi_{+\sigma_B}(x^-) \\
&\quad - \frac{e^2A_i}{cM_{AB}}\chi_{+\sigma_B}^{\dagger}(x^+)\chi_{+\sigma_B}(x^-) \\
&\quad + \frac{e\hbar}{2M_{AB}}\left[\vec{\nabla}\times\chi_{+\sigma_B}^{\dagger}(x^+)\vec{\sigma}\chi_{+\sigma_B}(x^-)\right]_i, \quad i=1,2.
\end{aligned}
\tag{8}
$$

Here,

$$
x^{\pm} = x\pm\varepsilon, \quad x = \left\{\vec{r},\ t_0\right\}, \quad \vec{r} = \{x,y\}, \quad t_0 = 0, \quad \varepsilon\to 0;
\tag{9}
$$

$v_{x^+x^-}^i$ is the velocity operator determined by a derivative of the Hamiltonian (1), $\chi_{+\sigma_B}(x^+)$ is the secondary quantized fermion field, the terms j_i^O, j_i^{Zb}, j_i^{so}, $i=x,y$ describe an ohmic contribution that satisfies the Ohm's law and contributions of the polarization and magneto-electric effects, respectively.

To perform quantum-statistical averaging for the case of nonzero temperature, we use a quantum-field method developed in references [32, 33]. After tedious but simple algebra one can find the conductivity in our model:

$$
\begin{aligned}
&\sigma_{ii}^O(\omega,\ k) \\
&= \frac{ie^2\overline{\beta}^2}{(2\pi c)^2}\operatorname{Tr}\int\left(1 - M_{BA}\left(\vec{p}\right)\frac{\partial^2 M_{BA}}{\partial p_i^2}\right) \\
&\quad \times\left(M\vec{v}^i(p), N\vec{v}^i(p)\right)d\vec{p},
\end{aligned}
\tag{10}
$$

$$
\begin{aligned}
&\sigma_{ll}^{Zb}(\omega,k) = \frac{ie^2}{\overline{\beta}^2(2\pi c)^2} \\
&\quad \times\operatorname{Tr}\int\frac{M_{BA}\left(\vec{p}\right)}{2}\sum_{i=1}^{2}\frac{\partial^2 M_{BA}}{\partial p_i^2}\left(M\vec{v}^i(p), N\vec{v}^i(p)\right)d\vec{p},
\end{aligned}
\tag{11}
$$

$$
\begin{aligned}
&\sigma_{12(21)}^{so}(\omega,k) = (-1)^{1(2)}\frac{i}{2}\frac{ie^2\overline{\beta}^2}{(2\pi c)^2} \\
&\quad \times\operatorname{Tr}\int M_{BA}\left(\vec{p}\right)\frac{\partial^2 M_{BA}}{\partial p_1\partial p_2}\left(M\vec{v}^{1(2)}(p), N\vec{v}^{1(2)}(p)\right)\sigma_z d\vec{p}
\end{aligned}
\tag{12}
$$

for the current j_i^O, j_i^{Zb}, j_i^{so}, respectively. Here, matrices M, N are given by the following expressions:

$$
M = \frac{f\left[\overline{\beta}((H(p^+)-\mu)/\hbar)\right] - f\left[\overline{\beta}\big(H^{\dagger}(-p^-)-\mu/\hbar\big)\right]}{\overline{\beta}z - \overline{\beta}(H(p^+)/\hbar) + \overline{\beta}(H^{\dagger}(-p^-)/\hbar)},
$$

$$
N = \frac{\delta(\hbar\omega+\mu)}{\left(\hbar z + H(p^+) - H^{\dagger}(-p^-)\right)\overline{\beta}}.
$$

Here, f is the Fermi–Dirac distribution, $z = \omega + i\varepsilon$, $\vec{p}^{\pm} = \vec{p} \pm \vec{k}$, ω is a frequency, μ is a chemical potential, and $\overline{\beta}$ is an inverse temperature divided by c.

5. Method of conductivity calculation

5.1 Diagonalized representation of the Hamiltonian

We perform the conductivity calculation in a representation where the Hamiltonian of the graphene model is diagonalized to find the velocity determined in the following way:

$$\vec{v}_{AB} \approx \frac{\partial H_{AB}}{\partial \vec{p}}. \tag{13}$$

The velocity operator $\vec{v}_{AB(BA)}$ should be transformed by the transformation of the form $S^{-1}\vec{v}_{AB}S$ with a matrix S constructed on the eigenvectors χ of the Hamiltonian. The corresponding matrix S should be constructed on the eigenvectors of the operator adjoined to the Hamiltonian. In every p-point the particle (hole) Hamiltonian is represented by 2×2 matrix, we denote matrix elements of the exchange operator $\left(i\Sigma^x_{rel}\right)_{AB(BA)}$ formally as $\Sigma^{AB(BA)}_{ij}$. Then, the eigenvectors χ_i, $i = 1, 2$ of the Hamiltonian (1) being the rows of the appropriate matrix S can be expressed in an explicit way:

$$\chi_1 = \left\{ \frac{ip\sin(\phi)\left(\Sigma^{AB}_{11}\Sigma^{AB}_{21} + \Sigma^{AB}_{12}\Sigma^{AB}_{22}\right) + p\cos(\phi)\left(\Sigma^{AB}_{12}\Sigma^{AB}_{22} - \Sigma^{AB}_{11}\Sigma^{AB}_{21}\right) - p\left(\Sigma^{AB}_{12}\Sigma^{AB}_{21} - \Sigma^{AB}_{11}\Sigma^{AB}_{22}\right)}{p\left(\left(\left(\Sigma^{AB}_{11}\right)^2 - \left(\Sigma^{AB}_{12}\right)^2\right)\cos(\phi) - i\left(\left(\Sigma^{AB}_{11}\right)^2 + \left(\Sigma^{AB}_{12}\right)^2\right)\sin(\phi)\right)}, 1 \right\}$$

$$\tag{14}$$

$$\chi_2 = \left\{ \frac{ip\sin(\phi)\left(\Sigma^{AB}_{11}\Sigma^{AB}_{21} + \Sigma^{AB}_{12}\Sigma^{AB}_{22}\right) + p\cos(\phi)\left(\Sigma^{AB}_{12}\Sigma^{AB}_{22} - \Sigma^{AB}_{11}\Sigma^{AB}_{21}\right) + p\left(\Sigma^{AB}_{12}\Sigma^{AB}_{21} - \Sigma^{AB}_{11}\Sigma^{AB}_{22}\right)}{p\left(\left(\left(\Sigma^{AB}_{11}\right)^2 - \left(\Sigma^{AB}_{12}\right)^2\right)\cos(\phi) - i\left(\left(\Sigma^{AB}_{11}\right)^2 + \left(\Sigma^{AB}_{12}\right)^2\right)\sin(\phi)\right)}, 1 \right\}$$

$$\tag{15}$$

In this way, we can calculate numerically the velocity operator in every p-point with subsequent its substitution to the conductivity integral.

5.2 Integral calculations

Contributions to conductivity include 2D integrals over the Brillouin zone (BZ). For example, the integrals in the ohmic contribution given by formulae (10) have the following form:

$$\sigma^{intra}_{ij}\left(\omega, \vec{k}\right) = \sum_{a=1,2} \frac{ie^2 v_0^2}{\pi^2} \int_{BZ} d^2\vec{p}\, \frac{\left(\left[v^i_{aa}(\vec{p})v^j_{aa}(\vec{p})\right]f\left[\varepsilon_1\left(\vec{p} - \vec{k}/2\right)\right] - f\left[\varepsilon_1\left(\vec{p} + \vec{k}/2\right)\right]\right)}{\left(\varepsilon_1\left(\vec{p} + \vec{k}/2\right) - \varepsilon_1\left(\vec{p} - \vec{k}/2\right)\right)\left(\omega - \varepsilon_1\left(\vec{p} + \vec{k}/2\right) + \varepsilon_1\left(\vec{p} - \vec{k}/2\right)\right)},$$

$$\tag{16}$$

$$\sigma_{ij}^{inter}\left(\omega,\vec{k}\right) = \frac{2i\omega e^2 v_0^2}{\pi^2} \int_{BZ} d^2\vec{p}\, \frac{v_{12}^i\left(\vec{p}\right)v_{21}^i\left(\vec{p}\right)\left(f\left[\varepsilon_1\left(\vec{p}-\vec{k}/2\right)\right] - f\left[\varepsilon_2\left(\vec{p}+\vec{k}/2\right)\right]\right)}{\left(\varepsilon_2\left(\vec{p}+\vec{k}/2\right) - \varepsilon_1\left(\vec{p}-\vec{k}/2\right)\right)\left(\omega^2 - \left(\varepsilon_2\left(\vec{p}+\vec{k}/2\right) - \varepsilon_1\left(\vec{p}-\vec{k}/2\right)\right)^2\right)}.$$

$$(17)$$

Here, the first integral is for the intraband transitions, and the second one is for the interband ones. Now, we highlight the pole structure for the integrands for small but finite $\vec{k}$, accounting for that $\varepsilon_1\left(\vec{p}\right) = -\varepsilon_2\left(\vec{p}\right)$. The first integral can be rewritten as:

$$\sigma_{ij}^{intra}\left(\omega,\vec{k}\right) = \sum_{a=1,2} \frac{ie^2 v_0^2}{\pi^2} \int_{BZ} d^2\vec{p}\left[v_{aa}^i\left(\vec{p}\right)v_{aa}^j\left(\vec{p}\right)\right]\frac{df(\varepsilon)}{d\varepsilon}\Bigg|_{\varepsilon=\varepsilon_1\left(\vec{p}\right)}\frac{1}{\left(\omega - \vec{k}\cdot\nabla\varepsilon_1\left(\vec{p}\right)\right)},$$

$$(18)$$

where we have performed the Taylor series expansion on $|\vec{k}|$ up to linear terms. In the second integral, only the second term in the denominator can produce poles, so we expand it into a power series on $|\vec{k}|$, making a change to polar coordinates $\left(p_x, p_y\right) \rightarrow (p,\phi)$ that results:

$$\sigma_{ij}^{inter}\left(\omega,\vec{k}\right) = \frac{2i\omega e^2 v_0^2}{\pi^2} \int_{BZ} pdpd\phi\, \frac{v_{12}^i\left(\vec{p}\right)v_{21}^i\left(\vec{p}\right)\left(f\left[\varepsilon_1\left(\vec{p}-\vec{k}/2\right)\right] - f\left[\varepsilon_2\left(\vec{p}+\vec{k}/2\right)\right]\right)}{\left(\varepsilon_2\left(\vec{p}+\vec{k}/2\right) - \varepsilon_1\left(\vec{p}-\vec{k}/2\right)\right)\left(\omega^2 - 4p^2 - k^2\sin^2\phi\right)}.$$

$$(19)$$

Pole structure of (18) and (19) is presented in **Figure 3**. In accordance with Eq. (18) and **Figure 3** at $\vec{k} = 0$ this integral is a regular one, whereas at finite k there is a line of poles (dashed lines in the **Figure 3**). At a finite k the pole structure of $\sigma_{ij}^{inter}\left(\omega,\vec{k}\right)$ (19) is an elliptic one that results in the necessity to account for an infinite sum of poles as a contribution to conductivity: $\sigma_{ij}^{inter}\left(\omega,\vec{k}\right) \propto \int d\phi\ \mathrm{Re}\, s(\phi)$, where $\mathrm{Re}\, s(\phi)$ is a residue in the pole located at angle ϕ on the poles line. The integral (19) in the case $k=0$ holds poles laying at a circumference that can be effectively reduced to a single one as $\sigma_{ij}^{inter}\left(\omega,\vec{k}\right) \propto 2\pi\ \mathrm{Re}\, s_1$, where $\mathrm{Re}\, s_1$ is a residue in arbitrary point of the circumference. For every oblate ellipse at large wave numbers, k, the main contribution to the integral (19) gives the only points touching the circumference $\sigma_{ij}^{inter}\left(\omega,\vec{k}\right) \sim 2\ \mathrm{Re}\, s_1$. Thus, the value of the optical conductivity decreases with the growth of k.

We define the upper integration limit for the model with linear dispersion in a way based on reasoning from the energy limit of tight-binding-approximation applicability ($\omega_{max} < 1$ eV $\approx 10^4$ K). Then, the upper integration limit q_{max} on momentum is $q_{max} \sim \omega_{max}/v_F$, $\omega_{max} < 1$ eV, and correspondingly for the massless Dirac fermions model, the integration should use the range from 0 to $|\vec{q}| < 0.14\,|\vec{K}_A|$. As the simulation results presented in **Figure 4** show the integration within this limit leads to the conductivity fall in the range $\omega_{max} \sim 4000$ K (0.3 eV) at the temperature of 3 K.

Thus, the range of momenta to predict conductivity in near-infrared and visible spectral ranges is outside the limits of applicability of the massless pseudo-Dirac fermion model.
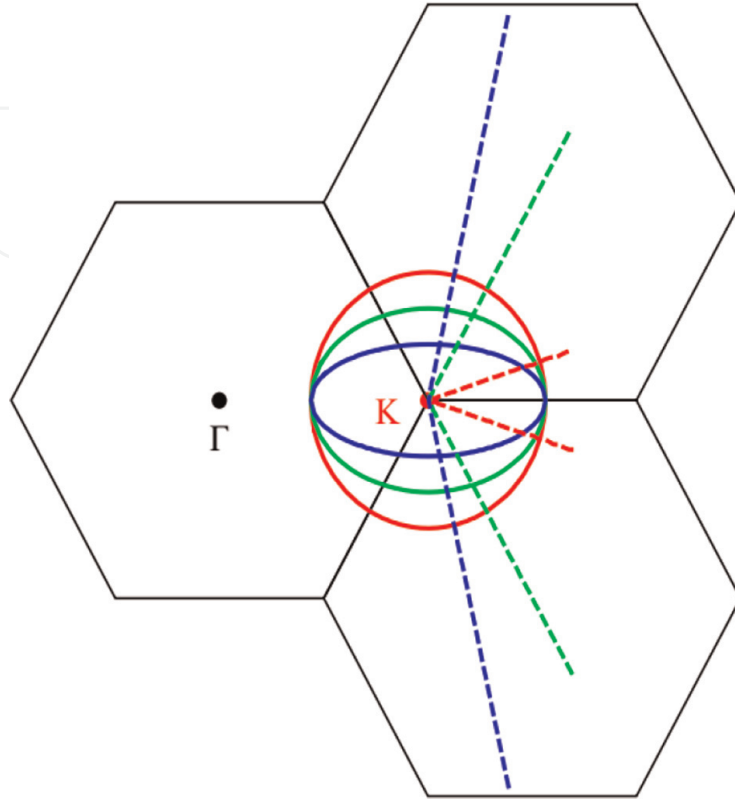

Figure 3.
Sketch of the poles structure of integrands for intra-(dashed lines) and inter-(solid lines) bands contribution to conductivity. Solid lines parameters at $\omega = 1$ (in units of $v_F |\vec{K}_A|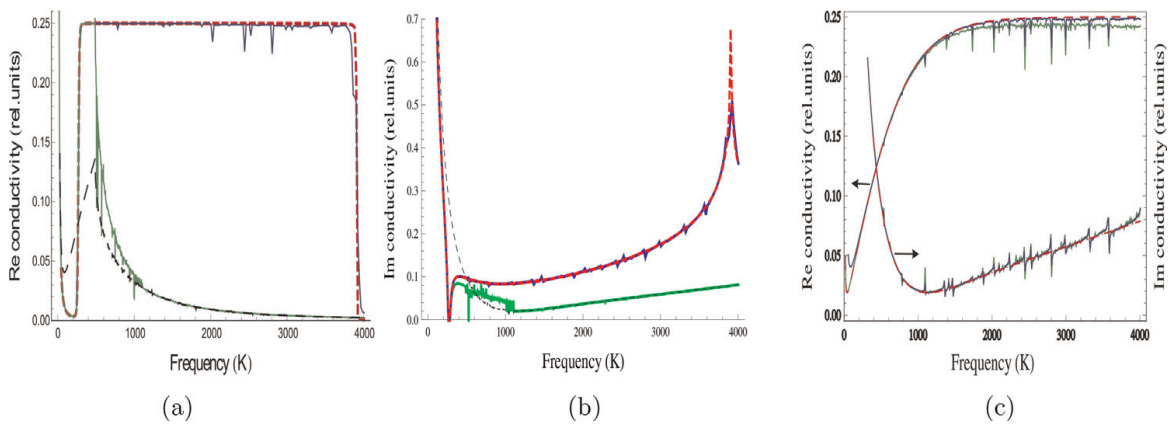$) are $k/|\vec{K}_A| = 0.1$ (red), 0.7 (green), 0.9 (blue). Dashed line parameters at $\omega = 0.2$ (in units of $v_F |\vec{K}_A|$) are $k/|\vec{K}_A| = 0.21$ (red), 0.4 (green), 0.9 (blue).

Figure 4.
Frequency dependencies of the real and imaginary parts of the massless ohmic term of conductivity at very small wave number $q = 10^{-8}|\vec{K}_A|$ in relative units of $e^2/\hbar$; a cutting parameter $q_{max} = 0.14\ |\vec{K}_A|$. The model [9, 32] is simulated at $T = 3$ K, chemical potential $\mu = 135K$ (red-dashed lines in figures (a–b)) and at $T = 200$ K, $\mu = 33$ K (red-dashed line in figure (c)). Numerical results for our model are green-solid and black-dashed lines for the approximation with zero gauge phases at $T = 3$ K, $\mu = 135K$ and $T = 200$ K, $\mu = 33K$, respectively, and blue line for the approximation with nonzero gauge phases at $T = 3$ K, $\mu = 135K$ in figures (a–b). (c) Dependence of the real and imaginary parts of the massless ohmic term of conductivity on the damping γ for the approximation of the nonzero gauge fields with $\gamma = 0.1$ (green curve) and $\gamma = 1$ (blue curve) at $T = 200$ K, $\mu = 33K$.

According to our calculation presented in **Figure 1c**, the energy bandstructure is flattened for the pseudo-Majorana fermion graphene model. It signifies that the Fermi velocity v_M for our model pseudo-Majorana states tends to zero for high wave numbers q. Since $v_M \to 0$ for large q the applicability condition $v_M q < \omega_{max}$ holds always. We choose $|\vec{q}| \leq 0.38|\vec{K}_A|$ as the limit of integration over momentum $|\vec{q}|$ because it is in the range of $|\vec{q}|$ from $0.28|\vec{K}_A|$ to $0.56|\vec{K}_A|$ appropriate for our model. Such choice corresponds to $\omega_{max} > 7000$ K.

In the approximation with zero-phases of the gauge fields, the analytical formulas for the integrands in the conductivity contribution terms have been used. The integrals have been calculated with adaptive integration steps in both directions ($|k|, \phi$) providing high calculation accuracy (not less than 0.01%).

In the approximation with nonzero gauge fields, we have to calculate numerically by introducing into consideration the small-positive damping constant γ for the states as a small imaginary contribution to the energies. The values of γ define the extent of smoothness of the singular behavior of the integrand and does not influence the general form of the dependency curve in accordance with **Figure 4c**.

All quantities necessary for the calculation of the complex conductivity have been calculated on a grid in the space of wave vectors with 200-point discretization in the angle ϕ for every given wave number q and variable step (a denser grid at small wave numbers and larger at large ones) to the maximum wave number $q_{max} = 0.38|\vec{K}_A|$. The 2D interpolation on this grid has been used for integrands evaluation in the intermediate points that are necessary for conductivity simulations. An error stipulated by the interpolation from the grid in wave vectors space has been roughly estimated by interpolation of the conic spectrum of the Dirac pseudo-fermion model on the same lattice with subsequent usage of the interpolation data for evaluation of the conductivity. Its value turns out to be less than 10^{-3}%.

Total estimation of the conductivity error has been performed by variation of the number of points used for interpolation of the energy band spectrum (by diminishing this number at factor two and subsequent comparison of the simulation results in both cases). It turns out to be not exceeding 10% in the considered frequency region. It should be noted that the error bars for values of the Fermi velocity that were measured by different techniques, including transport experiments (Shubnikov–de Haas oscillations) [34], infrared measurements of the Pauli blocking in graphene [35], magneto-optics [36], were also of the order of 10%.

6. Far-infrared optical spectroscopy of graphene

In this section, we study optical transitions in the Majorana-like fermion graphene model and compare the theoretical predictions with experimental data for the far-infrared spectral range. The frequency dependencies of the real and imaginary part of the ohmic optical conductivity ($\left|\vec{k}\right| = 0$) for temperatures $T = 3, 200$ K are shown in **Figure 5**. Chemical potentials, μ, are used to be 135 and 33 K for $T = 3$ and 200 K, respectively. For comparison, far-infrared conductivity is shown in the pseudo-Dirac fermion graphene model [9].

The conductivity in the far-infrared spectral range calculated within the massless pseudo-Dirac fermion graphene model gains a constant value that contradicts the experimental data.

(a)

(b)
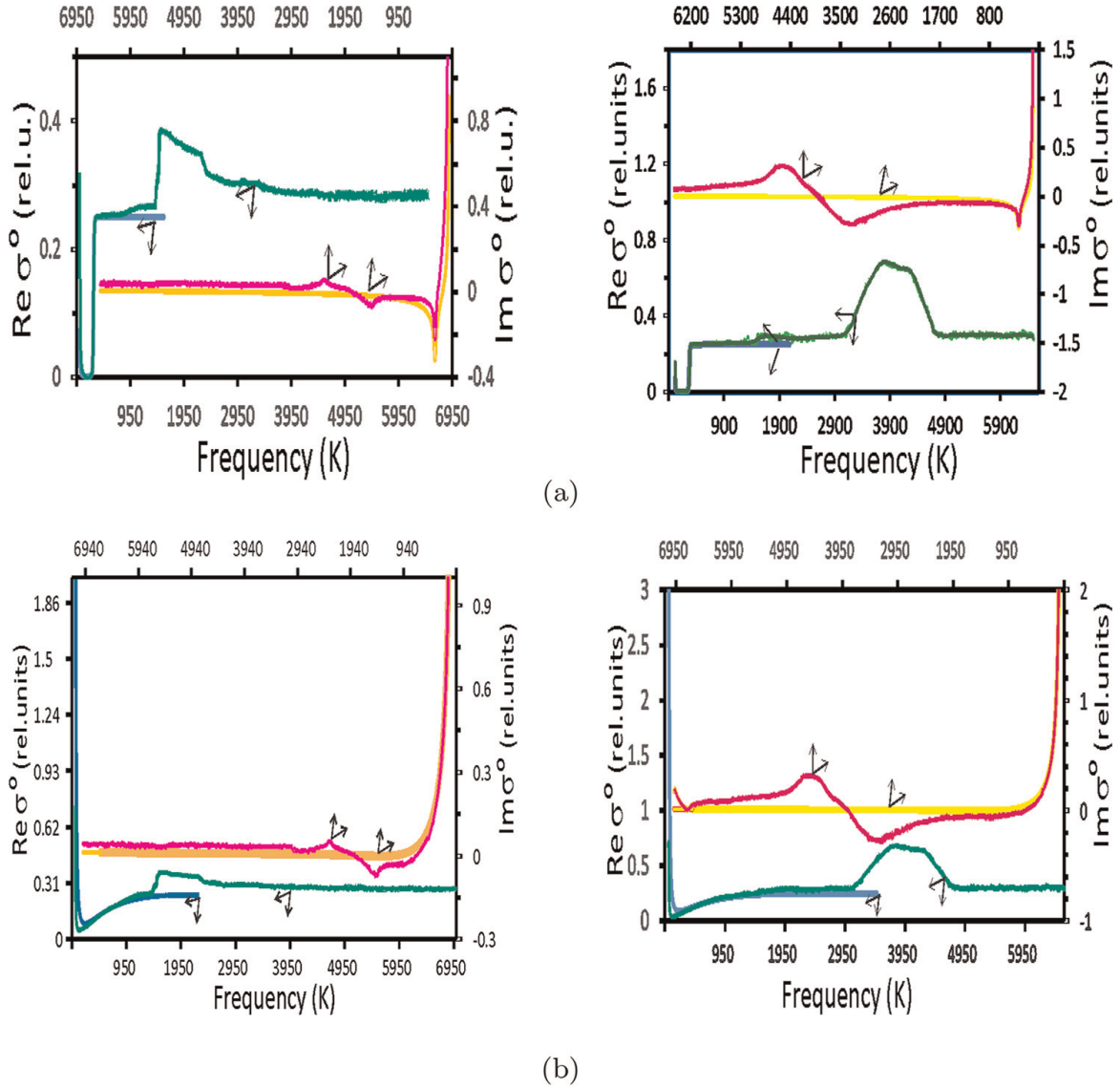
Figure 5.
Frequency dependencies of real (green and blue solid lines) and imaginary (yellow and magenta solid lines) parts of ohmic contribution $\sigma^{O}_{xx(yy)}$ to the far-infrared conductivity in relative units of $e^2/\hbar$ for our model (1) (green and magenta lines) and for the Dirac massless fermion model [9, 32] (blue and yellow lines). The calculations were carried out at temperatures $T = 3$ (a), $200(b)$ K and chemical potentials $\mu = 135$ (a), $33(b)$ K for two case: Taking into account (left) and neglecting (right) the pseudo-Majorana mass term.

The real part of the ohmic contribution in the optical conductivity for the pseudo-Majorana fermion graphene model undergoes a steep increase finalizing a much slower fall in the spectral range of $1000 - 2000$ K (see **Figure 5**, left). The maximum conductivity is at the frequency of~ 2000 K (0.13 eV). The predicted presence of the asymmetric spectral band in the optical conductivity for graphene is confirmed experimentally that the asymmetric peak is really observed on a frequency of ~ 0.15 eV ($\sim 150 - 200$ cm^{-1})[10].

The slow decrease of the peak intensity compared to the rise finalizes with steep achieving the plateau, which in turn ends with a shallow minimum in the remaining higher-frequency part of the far-infrared spectrum shown in **Figure 5**, left. Verifying the prediction of low (antipeak) being on the frequency of ~ 0.27 eV (3000 K) the experiment [12] confirms that the experimental antipeak is really indicated in the spectral range of $\sim 0.2 - 0.3$ eV.

The appearance of the peak is accompanied by the tendency of the imaginary part of the ohmic contribution in the optical conductivity toward negative values. It testifies that the position of the peak in the real part correlates with the emergence of plasmon oscillations. The exclusion of the pseudo-Majorana mass term results in the loss of the asymmetry of the far-infrared conductivity peak and a shift to the high-frequency region (see **Figure 5**, right). It testifies that chiral symmetry is restored, and correspondingly the anomalous transport disappears. According to results presented in **Figure 5**, the far-infrared peak and antipeak exist at both low and high temperatures. The influence of temperature consists in their smoothing, which impedes their experimental detection.

7. Electronic transport and field effect

In this section, we study essential features of the electric charge transport by Majorana-like carriers in graphene and compare theoretical predictions with experimental data.

Total current $\vec{J}$ in graphene is determined by electron and hole currents of valleys K, K' as $\vec{J} = \vec{J}_K - \vec{J}_{K'}$. The two currents flow on non-coinciding paths in the topologically nontrivial pseudo-Magorana graphene model because the jump of an electron (hole) from a site of sublattice A (B) to the nearest site of sublattice B (A) is equivalent to bypassing the lattice site with the acquisition of the carrier wave function of the phase, being a multiple of the group generator $\pi 6$ of the homotopy group $\mathbf{Z}_{12}$ (**Figure 2**) in addition to 60-degree rotation by virtue of the homotopy group of graphene Brillouin zone and the hexagonal symmetry. It signifies that at transition from one trigonal sublattice to another one, the direction of motion of the charge carrier is rotated at an angle of $\frac{\pi}{2}$. As a result, the $\vec{J}_K, \vec{J}_{K'}$ are orthogonal.

Let us denote the first and the second terms in the conductivity σ_{ii}^O (see Eq. 10) through σ_{ii}^o and σ_{ii}^{add}, respectively: $\sigma_{ii}^O = \sigma_{ii}^o + \sigma_{ii}^{add}$. σ_{ii}^{add} and σ_{ii}^o depend and do not depend on the Majorana-like mass term M_{AB}, respectively. Then, taking into account of the polarization effects (Eq. 11) one can determine the pseudo-Majorana corrections, σ_{ii}^{tp}, $i = x, y$ to the conductivity in the following way: $\sigma_{ii}^{tp} = \sigma_{ii}^{add} + \sigma_{ii}^{Zb}, \sigma_{xx}^{tp} = -\sigma_{yy}^{tp}$.

Then, in the absence of the Majorana conductivity corrections, we get the Ohm's law because of the direction of the sum, $\vec{J}^o = \vec{J}_K^o - \vec{J}_{K'}^o$ of the currents, $\vec{J}_K^o, \vec{J}_{K'}^o$, equal to $\mathfrak{Re}\ \sigma_{ii}^o \vec{E}_i, i = x, y$ coincides with the direction of an applied electric field $\vec{E}, \vec{E} = \vec{E}_x + \vec{E}_y$ as **Figure 6** shows. Meanwhile, the direction which is orthogonal to $\vec{E}$ the current is absent. Taking into account the pseudo-Majorana conductivity corrections, the total current changes in the following way: $\vec{J}_{skew} \equiv \vec{J}_K - \vec{J}_{K'} = \vec{J}^o + \sigma_{xx}^{tp}\vec{E}_x - \sigma_{yy}^{tp}\vec{E}_y \equiv \sum_{i=1}^{2}(-1)^{i-1}(\sigma_{ii}^O + \sigma_{ii}^{Zb})\vec{E}_i$. As **Figure 6** shows the $\vec{J}_{skew}$ is rotated in respect to $\vec{E}$, and correspondingly a nonzero component of the current appears in the direction orthogonal to $\vec{E}$. It proves that a topological current can exist in the pseudo-Majorana graphene model and the abnormal transport appears due to the presence of the Majorana mass term.

Figure 7 demonstrates negative differential conductivity for the topological current $J^{tp} = \mathfrak{Re}\sigma_{ii}^{tp}(\omega)U$ assuming the increase of the system energy in a form $\hbar\omega \sim U^2$, where U is a bias voltage.

A total spin-orbital valley current $\vec{J}_{VHE} = \sigma^{so}_{xy}\vec{B}_y - \sigma^{so}_{yx}\vec{B}_x$ is produced under an action of a magnetic field $\vec{B}_\parallel$ parallel to $\vec{E}$. One can note that $\vec{J}_{VHE}$ is always directed tangentially to the bias $\vec{E}$ and added to the current $\vec{J}^{tp}$. Then, the total current in the
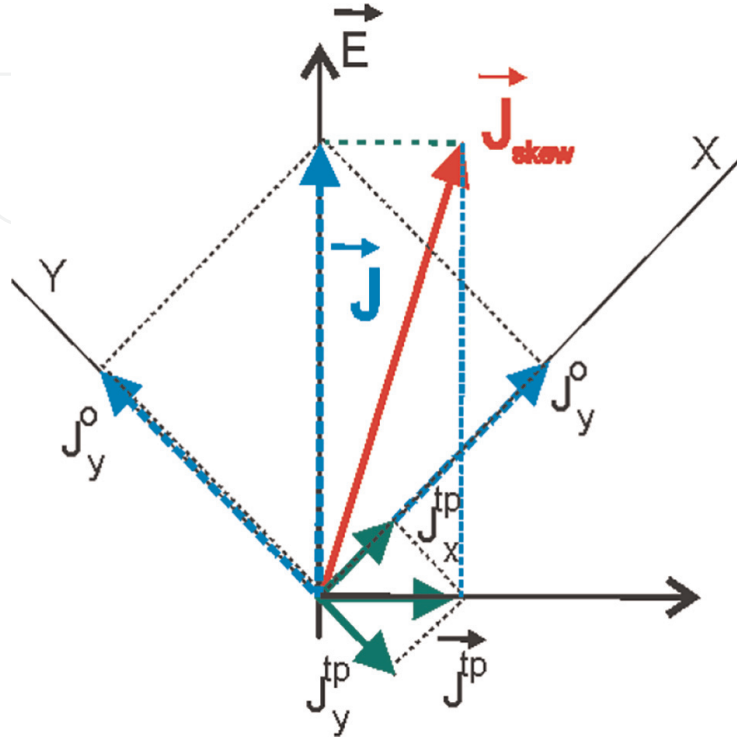

Figure 6.
Sketch of currents in the topologically nontrivial semimetal: $J^o_{x(y)}$ is a massless ohmic current along the axis $X(Y)$, J^{tp} is a sum, $\sum_{i=1}^{2}\left(\sigma^{add}_{ii} + \sigma^{Zb}_{ii}\right)\vec{E}_i$ of the polarization and dynamical-mass corrections to $J^o_{x(y)}$. $\vec{E}$ is an applied electric field.
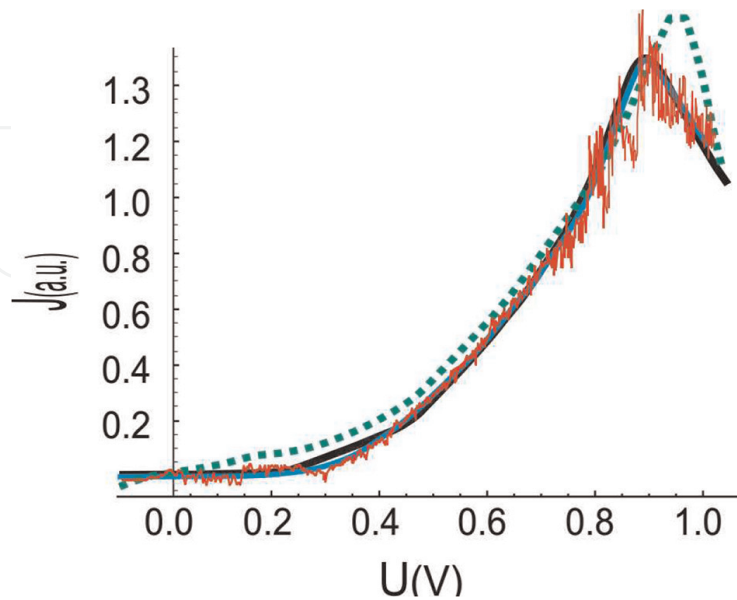

Figure 7.
Dependencies of topological current J on bias voltage U: Simulation results (red solid curve) and their fitting (blue solid curve) for negative differential conductivity (NDC) in our quasi-relativistic graphene model at temperature T = 3 K, chemical potential μ = 135 K; black solid and green dashed curves present experimental data and theoretical calculation for NDC in two graphene flakes twisted approximately at 90° to each other at 1.8° misalignment angle [37]. The bias voltage U is given in volts "V."

direction of the vector $\vec{E}$ increases. It signifies that a negative magnetoresistance (NMR) appears at weak magnetic fields parallel to electric ones. NMR is a specific feature of topological materials and presents a phenomenon of chiral anomaly [38, 39].

Let us investigate longitudinal conductivity for low frequencies $\omega \to 0$ and non-vanishing wave vectors $\vec{k} = \vec{p}/\hbar - \vec{K}_{A(B)}$. The longitudinal conductivity $\sigma_L\left(\omega, \vec{k}\right)$ is determined through the conductivity tensor splitting into longitudinal and transversal terms as [40]

$$\sigma_{ij}\left(\omega, \vec{k}\right) = \left(\delta_{ij} - \frac{k_i k_j}{\vec{k}^2}\right)\sigma_T\left(\omega, \vec{k}\right) + \frac{k_i k_j}{\vec{k}^2}\sigma_L\left(\omega, \vec{k}\right); i, j = x, y. \tag{20}$$

when choosing $\vec{k} = (k_x, 0)$, $\vec{k} = (0, k_y)$, or $k_x = k_y = k$ one always has:

$$\sigma_{xx}\left(\omega, \vec{k}\right) = \sigma_L(\omega, k), \quad or \, \sigma_{yy}\left(\omega, \vec{k}\right) = \sigma_L(\omega, k).$$

Now, let us calculate the low-frequency conductivity $\sigma\left(\omega, \vec{r}\right)$. To do it, one has to perform the inverse Fourier transformation.

$$\sigma\left(\omega, \vec{r}\right) = \frac{1}{(2\pi)^2}\int \sigma_L^o(\omega, k)e^{i\vec{k}\cdot\vec{r}}d^2k. \tag{21}$$

Here, ω is a cyclic frequency. We consider the effects of spatial dispersion on the real part $\Re e \; \sigma_L^O(\omega, k)$ of the longitudinal complex conductivity at the low frequencies: $\omega = 10^{-10}$, 0.004, 13.3 K (kelvin) for the massless pseudo-Dirac graphene fermion model with the number of flavors $N_F = 2$ (pseudospin and spirality) and our graphene model with the $N_F = 3$ flavors. Conductivity for frequencies in the Hertz range, for example, 2.08 Hz ($\omega = 10^{-10}$ K), can be considered as a minimum conductance for direct current. The numerical results are presented in **Figure 8**.

The function $\Re e \; \sigma_L^o(\omega, k)$ for the massless pseudo-Dirac fermion graphene model is a positive constant function. The $\Re e \sigma_L^o(k)\big|_{k\to\infty} \equiv \Re e \; \sigma_{k_\infty}$ is the positive constant ($\Re e \; \sigma_{k_\infty} > 0$) for the all frequencies (it is equal to ~ 0.004 for $\omega = 0.004, 10^{-10}$ K and ~ 0.017 for $\omega = 13.3$ K. The real part of the longitudinal complex conductivity in the $N_F = 2$-model becomes the very large positive constant, $\Re e \; \sigma_L^o(k)\big|_{k\to 0} \equiv \Re e \; \sigma_{k_0} \sim$ 44.443, at small values of k, $k \ll 1$ for the frequencies $\omega = 10^{-10}$, 0.004 K. As **Figure 8** shows the function $\Re e \; \sigma_L^o(\omega, k)$ in the $N_F = 2$-model sharply increases in a very narrow range of k/K_A. Since $\Re e \; \sigma_L^o(\omega, k)$ is constant almost everywhere for the $N_F = 2$-model of graphene does not oscillate and $e^{i\vec{k}\cdot\vec{r}}$ enters the integrand of the expression (21), the $\Re e \; \sigma\left(\omega, \vec{r}\right)$ is equal to zero, and correspondingly the minimum conductivity is equal to zero in this graphene model. But this prediction for the DC case contradicts the experimental facts that the value of the low-frequency conductivity is in the range $4\frac{e^2}{h} - 6\frac{e^2}{h}$.

The function $\Re e \; \sigma_L^o(\omega, k)$ for the pseudo-Majorana graphene $N_F = 3$-models both with and without the pseudo-Majorana mass term is a sign-alternating one at $k \to \infty$. It signifies that the plasmon oscillations can emerge in the graphene $N_F = 3$-models.
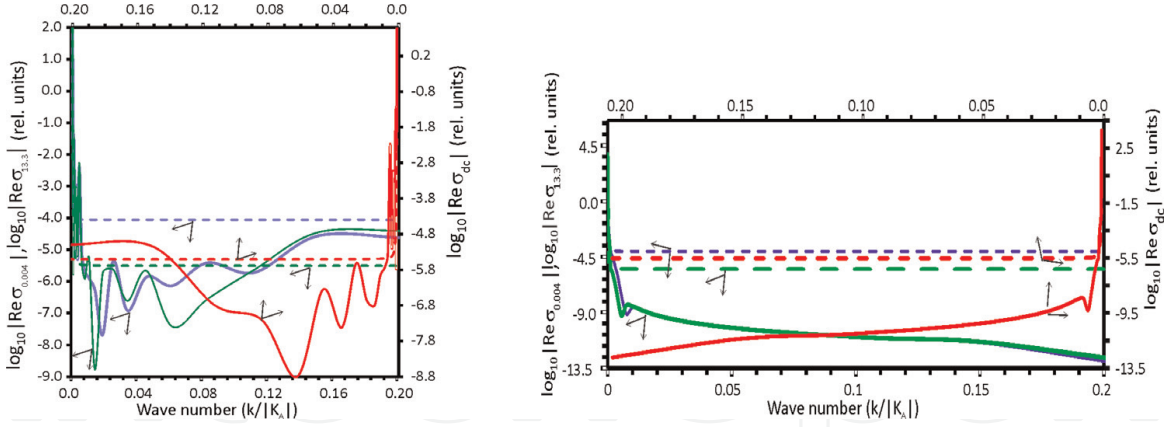
Figure 8.
Real part $\sigma_L^o(\omega, k)$ of the longitudinal ohmic contribution to conductivity vs. wave number k, $\vec{k} = \vec{p} - \vec{K}_{A(B)}$ for our pseudo-Majorana fermion $N_F = 3$-model (1) (solid curves) and for the massless Dirac fermion model [32] (dashed curves), at the frequencies ω: 13.3 K (0.27 THz, blue color), 0.004 K (83 MHz, green color), 10^{-10} K (2.08 Hz, red color). The calculations were carried out at temperatures $T = 100$ K and chemical potentials $\mu = 1$ K for two case: Taking into account (left) and neglecting (right) the pseudo-Majorana mass term. $\sigma_L^o(\omega, k)$ is measured in the relative units of e^2/h and labeled as $\Re e\ \sigma_{13.3}$, $\Re e\ \sigma_{0.004}$ and $\Re e\ \sigma_{dc}$ for the frequencies 13.3, 0.004, and 10^{-10} K, respectively.

Neglecting the pseudo-Majorana mass term the function $\Re e\ \sigma_L^o(\omega, k)$ for the pseudo-Majorana fermion graphene $N_F = 3$-model is weakly oscillating for all frequencies (see **Figure 8**). Since $\Re e\ \sigma_L^o(\omega, k)$ for this case is practically constant except for a very narrow interval, then as well as for the $N_F = 2$ model, the $\Re e\ \sigma\left(\omega, \vec{r}\right)$ is equal to zero, and correspondingly the graphene model with the chiral pseudo-Majorana charge carriers is not semimetal.

Now let us examine the $N_F = 3$ model with the nonzero pseudo-Majorana mass term. In this case, the $\Re e\ \sigma_L^o(\omega, k)$ strongly oscillates for all frequencies (**Figure 8**). In this case for $\omega = 0.004, 10^{-10}$ K, since the $\Re e\ \sigma_L^o(\omega, k)$ has the large maximum ($\sim 44.55 \frac{e^2}{h}$), and oscillating tends to zero it behaves like the function $\Re e\ \sigma_{k\,max}\ \frac{\sin(k - k_{\,max})}{(k - k_{\,max})}$. Such sort of functions can be considered as a finite approximation of the Dirac $\delta-$function in the form of the sinc function $\lim_{\varepsilon \to 0^+} \frac{\sin x}{\varepsilon x}$, and the coefficient $\Re e\ \sigma_{k\,max}$ is called the intensity or spectral power of the $\delta-$function. In the DC limit ($\omega = 10^{-10}$ K), the $\Re e\ \sigma_L^o(\omega, k)$ possesses one maximum at $k \to 0$. Correspondingly, the DC minimum conductivity $\sigma^{dc}\left(\vec{r}\right)$ for the $N_F = 3$ model with the chiral anomaly may be approximated by the integral with only one Dirac δ-function entering the integrand:

$$\sigma^{dc}\left(\omega, \vec{r}\right) = \frac{1}{(2\pi)^2} \int \Re e\sigma_L^o(\omega, k) e^{i\vec{k}\cdot\vec{r}} d^2k \approx \frac{1}{2\pi} \int \Re e\sigma_L^o(\omega, 0)\delta(k) e^{i\vec{k}\cdot\vec{r}} dk = \frac{7e^2}{h}, \quad \omega = 10^{-10} K.$$

(22)

The minimum DC-conductivity of graphene in devices with a large area of a graphene monolayer on SiO_2 turns out to be of $4e^2/h$ [4] at low temperatures (~ 1.5 K). The minimum DC-conductivity of suspended graphene [5, 6] and of graphene on boron nitride substrate [41] is of $\sim 6e^2/h$ at $T \sim 300$ K. Since for $\omega = 0.004$ K one obtains the same value of the conductivity the low-frequency conductivity behaves in

a universal manner. Thus, our estimate (22) is in perfect agreement with the experimental data.

8. Conclusion

To finalize our finding, within the earlier developed quasi-relativistic model of graphene, the frequency-dependent conductivity of graphene has been investigated theoretically in a number of experimentally interesting cases. It has been demonstrated that accounting of exchange interactions in the model which leads to its topological nontriviality both in electron structure and quasi-particle excitations not only modifies Ohmic conductivity dependencies both on frequency and temperature but also adds few contributions to conductivity stipulated by Majorana-like mass term corrections. Account of these corrections allows one to obtain a fine description of experimentally observable effects in graphene conductivity dependencies as in frequency domain as for knows unsolved problem of minimum DC-conductivity.

Author details

Halina V. Grushevskaya and George Krylov
Physics Department, Belarusian State University, Minsk, Belarus

*Address all correspondence to: grushevskaja@bsu.by

IntechOpen

References

[1] Cooper DR, D'Anjou B, Ghattamaneni N, Harack B, Hilke M, Horth A, et al. Experimental review of graphene. ISRN Condensed Matter Physics. **2012**;**2012**:501686

[2] Pippard AB. Magnetoresistance in Metals. Cambridge: Cambridge University Press; 2009

[3] Hayes IM, Maksimovic N, Lopez GN, Chan MK, Ramshaw BJ, McDonald RD, et al. Superconductivity and quantum criticality linked by the hall effect in a strange metal. Nature Physics. 2021;**17**:58

[4] Novoselov KS, Geim AK, Morozov SV, et al. Electric field in atomically thin carbon films. Science. 2004;**306**:666

[5] Bolotin KI, Sikes KJ, Hone J, Stormer HL, Kim P. Temperature-dependent transport in suspended graphene. Physical Review Letters. 2008;**101**:096802

[6] Du X, Skachko I, Barker A, Andrei EY. Approaching ballistic transport in suspended graphene. Nature Nanotechnology. 2008;**3**:491

[7] Ziegler K. Minimal conductivity of graphene: Nonuniversal values from the Kubo formule. Physical Review B. 2007;**75**:233407

[8] Ando T, Zheng Y, Suzuura H. Dynamical conductivity and zero-mode anomaly in honeycomb lattices. Journal of the Physical Society of Japan. 2002;**71**:1318-1324

[9] Falkovsky LA. Optical properties of graphene and IV–VI semiconductors. Physics–Uspekhi. 2008;**51**(9):887

[10] Ju L, Geng BS, Horng J, Girit C, Martin M, Hao Z, et al. Graphene plasmonics for tunable terahertz metamaterials. Nature Nanotechnology. 2011;**6**:630-634

[11] Mak KF, Shan J, Heinz TF. Seeing many-body effects in single- and few-layer graphene: Observation of two-dimensional saddle-point excitons. Physical Review Letters. 2011;**106**:046401

[12] Mak KF, Ju L, Wang F, Heinz TF. Optical spectroscopy of graphene: From the far infrared to the ultraviolet. Solid State Communications. 2012;**152**:1341

[13] Mak KF, Sfeir MY, Wu Y, Lui CH, Misewich JA, Heinz TF. Measurement of the optical conductivity of graphene. Physical Review Letters. 2008;**101**:196405

[14] San-Jose P, Lado JL, Aguado R, Guinea F, Fernández-Rossier J. Majorana zero modes in graphene. Physical Review X. 2015;**5**:041042

[15] Cao Y, Fatemi V, Fang S, Watanabe K, Taniguchi T, Kaxiras E, et al. Unconventional superconductivity in magic-angle graphene superlattices. Nature. 2018;**556**:43

[16] Gorbachev RV, Song JCW, Yu GL, Kretinin AV, Withers F, Cao Y, et al. Detecting topological currents in graphene superlattices. Science. 2014;**346**:448

[17] Elias DC, Gorbachev RV, Mayorov AS, Morozov SV, Zhukov AA, Blake P, et al. Dirac cones reshaped by interaction effects in suspended graphene. Nature Physics. 2012;**8**:172

[18] Wang J-R, Liu G-Z. Eliashberg theory of excitonic insulating transition

in graphene. Journal of Physics. 2011;**23**: 155602

[19] Grushevskaya HV, Krylov GG. Electronic structure and transport in graphene: QuasiRelativistic Dirac-Hartree-Fock self-consistent field approximation. In: Aliofkhazraei M et al., editors. Graphene Science Handbook: Electrical and Optical Properties. Vol. 3. USA, UK: Taylor and Francis Group, CRC Press; 2016

[20] Grushevskaya H, Krylov G. Massless Majorana-like charged carriers in two-dimensional semimetals. Symmetry. 2016;**8**:60

[21] Grushevskaya HV, Krylov GG. Low frequency conductivity in monolayer graphene model with partial unfolding of Dirac bands. International Journal of Modeling Physics. 2016;**30**:1642009

[22] Grushevskaya HV, Krylov GG. Increasing spin-orbital coupling at relativistic exchange interaction of electron-hole pairs in graphene. Semiconductors. 2018;**52**:1879

[23] Grushevskaya H, Krylov G. Vortex dynamics of charge carriers in the quasi-relativistic graphene model: High-energy $\vec{k} \cdot \vec{p}$ approximation. Symmetry. 2020; **12**:261

[24] Grushevskaya HV, Krylov GG. Non-abelian properties of charge carriers in a quasirelativistic graphene model. Semiconductors. 2020;**54**:1737-1739

[25] Grushevskaya H, Krylov G. Polarization in quasirelativistic graphene model with topologically non-trivial charge carriers. Quantum Reports. 2022;**4**:1

[26] Grushevskaya HV, Krylov GG, Kruchinin SP, Vlahovic B, Bellucci S.

Electronic properties and quasi-zero-energy states of graphene quantum dots. Physical Review B. 2021;**103**:235102

[27] Grushevskaya HV, Krylov G. Semimetals with Fermi velocity affected by exchange interactions: Two dimensional Majorana charge carriers. International Journal of Nonlinear Phenomenon in Complex System. 2015; **18**:266

[28] Grushevskaya HV, Krylov G, Gaisyonok VA, Serow DV. Symmetry of model N = 3 for graphene with charged Pseudo-excitons. International Journal of Nonlinear Phenomenon in Complex System. 2015;**18**:81

[29] Dyson F. Advanced Quantum Mechanics. Singapore: World Scientific Publishing; 2007

[30] Krylova H, Gursky L. Spin Polarization in Strongly Correlated Systems. Saarbrucken, Germany: LAP Lambert Academic Publishing; 2013

[31] Davydov AS. Quantum Mechanics. Moscow: Science; 1973

[32] Falkovsky LA, Varlamov AA. Space-time dispersion of graphene conductivity. European Physics Journal. 2007;**56**:281

[33] Grushevskaya HV, George Krylov VA, Gaisyonok. Non-abelian currents in quasi-relativistic graphene model: General theory. International Journal of Nonlinear Phenomenon in Complex System. 2018;**21**:153

[34] Elias DC, Gorbachev RV, Mayorov AS, Morozov SV, Zhukov AA, Blake P, et al. Dirac cones reshaped by interaction effects in suspended graphene. Nature Physics. 2011;**7**:701

[35] Li ZQ et al. Nature Physics. 2008;**4**: 532

[36] Chen Z-G, Shi Z, Yang W, Lu X, Lai HY, Wang F, et al. Observation of an intrinsic bandgap and Landau level renormalization in graphene/boron-nitride heterostructures. Nature. Communications. 2014;**5**:4461

[37] Mishchenko A, Tu JS, Cao Y, Gorbachev RV, Wallbank JR, Greenaway MT, et al. Twist-controlled resonant tunnelling in graphene/boron nitride/graphene heterostructures. Nature Nanotechnology. 2014;**9**:808

[38] Lu H-Z, Shen S-Q. Quantum transport in topological semimetals under magnetic fields. Frontiers of Physics. 2017;**12**(3):127201

[39] Niemann AC, Gooth J, Wu S-C, et al. Chiral magnetoresistance in the Weyl semimetal NbP. Scientific Reports. 2017;**7**:43394

[40] Kraeft WD, Kremp D, Ebeling W, Röpke G. Quantum Statistics of Charged Particle Systems. Berlin: Academie-Verlag; 1986

[41] Dean CR, Young AF, Meric I, et al. Boron nitride substrates for high-quality graphene electronics. Nature Nanotechnology. 2010;**5**:722